Macromolecular Regulation of the Material Properties of Biomolecular Condensates

Divya Kota[a] *and Huan-Xiang Zhou*[a,b,]*

[a]Department of Chemistry and [b]Department of Physics, University of Illinois at Chicago, Chicago, IL 60607, United States

AUTHOR INFORMATION

Corresponding Author

* E-mail: hzhou43@uic.edu

Supporting Information

Experimental section

1. Sample preparation. Poly-L-lysine (catalog # P2658), FITC-Ficoll70 (catalog # 51731), and fluorescein sodium salt (catalog # 46960) were purchased from Sigma-Aldrich; heparin (catalog # A1698), FITC-heparin (catalog # HRN1-FC-1), and Ficoll70 (catalog # 17031010) were purchased from Alfa Aesar, Nanocs, Inc., and GE healthcare, respectively. Condensate samples were prepared in a microcentrifuge tube by sequentially adding buffer (10 mM imidazole pH 7 with 0.01% NaN_3), 1 M KCl, Ficoll70 (and FITC-Ficoll70 if needed, at desired total concentration), heparin (and FITC-heparin if needed), and poly-L-lysine. The final concentrations of poly-L-lysine and heparin were 100 μM each. When FITC-heparin was present, its concentration was 10 μM and the unlabeled heparin concentration was correspondingly reduced to 90 μM. In measurements involving beads, unless otherwise indicated, the beads were 2 μm-diameter carboxylate-coated polystyrene beads (Polysciences, Inc. catalog # 18327-10). Some measurements were also conducted using 2.26 μm-diameter uncoated polystyrene beads (Spherotech, Inc. catalog # PP-20-10).

2. Morphology of pK:H condensates. Condensate samples (3-5 μL) were loaded to a custom sample chamber built by affixing a coverslip to a glass slide via double-sided Scotch tape. Once mounted to the sample stage in an inverted orientation, pK:H condensates at different Ficoll70 concentrations were allowed to settle completely on the coverslip. The bright-field camera in a LUMICKS C-Trap™ dual-trap optical-tweezers instrument was used to capture images of the settled condensates.

3. Local melting of condensates inside focused laser beams. pK:H condensate samples including FITC-heparin and Ficoll70 (0 to 200 g/L) were loaded into a sample chamber and placed on the sample stage of the C-Trap™ instrument until a majority of droplets settled over the coverslip. Then the trapping laser (1064 nm) was turned to 100%, the overall power was set to a low level (3-10%) that was just enough for the laser beams to trap and grow two separate droplets. The trap 1 split was adjusted around 50% to ensure that the two droplets grew to equal size (by scavenging nearby small droplets). The trap 1 split was then fixed at 50% and the two droplets

were held until all other droplets settled to the coverslip. Lastly the two droplets were subject to local melting by increasing the overall power of the laser beams. Specifically, the power of the laser beams was held alternatively at a baseline level (e.g., 10% for 0 Ficoll70) and at increasingly elevated levels (with increments of 5 percentage points), each for approximately 30 s. The entire process was recorded by both the bright-field camera (15 Hz frame rate) and a confocal detector. For the latter, the excitation wavelength was 488 nm, and the scanned area was around 40 μm × 20 μm (with pixel size at 0.2 μm and pixel dwell time at 0.05 ms). Additional local melting of pK:H condensates was conducted at 50 g/L Ficoll70, this time with a bead trapped in each laser beam.

4. Calibration of local temperature jump due to laser heating. As is well known, a local temperature jump occurs when water absorbs the energy of an infrared laser beam. We calibrated the local temperature jump caused by the trapping laser in the C-Trap™ instrument using the temperature dependence of the fluorescence intensity of fluorescein. An aliquot of 10 μM fluorescein (in deionized water) was placed on the sample stage. Confocal images were acquired both before the trapping laser was on and after it was evenly split between two beams with the power at 30%, 40%, 50%, and 100%. Care was taken to align the laser beams horizontally (along the *x* axis). The process was repeated when the two laser beams, kept at the same positions, each trapped a bead. The excitation wavelength was 488 nm (5% excitation laser power), and the emission band pass filter was 511/20 nm. The scanned area was 50 μm × 12 μm (with pixel size at 0.1 μm and pixel dwell time at 1 ms).

The fluorescence intensity profile with the trapping laser off, when divided by the highest reading among all the pixels, was used to remove any instrument distortion. Specifically, the fluorescence intensity profile at any given laser power was first normalized by the laser-off profile. The normalized fluorescence intensity profile in the presence of the laser beams without trapped beads was then fit to the following function:

$$FI(x,y) = FI_{25^{\circ}C}\left[1 - \frac{C}{\prod_{i=1}^{2}(1 + f_i(x,y)/w_i^2)^{\alpha}}\right] \quad [S1]$$

where $FI_{25^{\circ}C}$ denotes the fluorescence intensity far away from the laser beams (where the temperature is at 25 ºC), w_i measure the widths of the regions with significant temperature jumps,

$f_i(x,y) = (x - x_{ic})^2 + (y - y_c)^2$ with (x_{ic}, y_c) representing the centers of the two laser beams, and C and α are two other fitting constants. When the laser beams trapped beads, the beads excluded water and dye molecules, thereby both reducing the local heating and resulting in darkening in their cross sections. We accounted for the latter effect by adding a Gaussian function for each bead:

$$FI(x,y) = FI_{25^oC}\left[1 - \frac{C}{\prod_{i=1}^{2}(1 + f_i(x,y)/w_i^2)^{\alpha}} - \sum_{i=1}^{2} B_i e^{-f_i(x,y)/H_i^2}\right] \quad [S2]$$

The darkened regions of the bead cross sections allowed a precise determination of the laser beam centers, which were then fixed in all the fitting. For any given laser power, we focused our attention on the maximum of the heating-induced fluorescence reduction, which occurred either at the center of a laser beam when a bead was not trapped or at the surface of a trapped bead.

To convert the fluorescence reductions to temperature jumps, we measured the fluorescence intensities of 10 μM fluorescein over a range of temperatures on a FluoroMax-4 spectrofluorometer (HORIBA Scientific). A 100-μL aliquot was placed in a cuvette with 10 mm path length (STARNA; catalog # 26.100F-Q-10/Z20). To match the conditions of the confocal scanning, the excitation wavelengths were set at 488 ± 0.75 nm, and excitation was collected at 1-nm intervals from 501 to 521 nm (with a 1.5-nm window at each emission wavelength). Starting from 25 ºC, the temperature of the sample was increased at 10 ºC increments till 85 ºC; the fluorescence was measured with an integration of 0.1 s after 2 min equilibration. With triplicate measurements, the mean reduction in fluorescence intensity, FI/FI_{25^oC}, was fit to a quadratic function of temperature jump (ΔT) with an intercept of 1. The maximum of the heating-induced fluorescence reduction from each confocal scan was then fed to this quadratic function to obtain the corresponding temperature jump.

5. Turbidity assay. Turbidity assay was done on the FluoroMax-4 spectrofluorometer. The samples were 100 μL of pK:H condensates at 0 to 200 g/L Ficoll70. Excitation and emission wavelengths were both set at 380 ± 1 nm. Starting from 25 ºC, the temperature of each sample was increased at 5 ºC increments till 85 ºC, and then to a last temperature of 92 ºC, with 2 min equilibration after reaching each temperature. At each temperature, the absorbance was measured five times, each with a 0.05 s integration time, and the average was recorded.

For pK:H condensates at each Ficoll70 concentration, 3-6 replicate measurements were made. The absorbance as a function of temperature in each replicate measurement was buffer-subtracted and normalized. The mean absorbance (A) at each temperature and the standard error of the mean were calculated among the replicate measurements. The mean melting curve was fit to the following function:

$$A(T) = \frac{1}{1 + (T/T_m)^{\beta}} \quad [S3]$$

where T and T_m are the temperature and melting temperature (both in ºC).

6. Partition coefficient of Ficol70 in pK:H condensates. Ficoll70 partition into pK:H condensates was assessed using FITC-Ficoll70 (5 μM) along with 100 g/L unlabeled Ficoll70. Confocal scans were made with the excitation wavelength at 488 nm (1% excitation laser power) and over an area around 50 μm × 40 μm (pixel size at 0.05 μm and pixel dwell time at 0.05 ms). The fluorescence intensities over a circular region of interest were measured both inside and outside pK:H condensates. The ratio of the inside and outside intensities was used as an estimate of the partition coefficient.

7. Measurements of interfacial tension and viscoelasticity. These measurements were done on the C-Trap™ instrument, as described previously [1]. In brief, the measurement of interfacial tension involved stretching a suspended droplet by pulling apart two polystyrene beads trapped at the poles of the droplet. As trap 1 was pulled at a constant speed (set at 0.05 μm/s) from trap 2, the forces at both traps increased linearly over time. The ratio between the sum of the force rates and the actually pulling speed (slightly lower than the set value) yielded the spring constant (χ_{sys0}) of the system of three effective springs in series: trap 1, the droplet, and trap 2. The system spring constant along with the stiffnesses of the two traps allowed the spring constant (χ_0) of the droplet to be determined. Finally the interfacial tension was found as [2]

$$\gamma = \frac{1}{\pi}\left[\ln\left(\frac{R}{a} - 1\right) + 0.68\right]\chi_0 \quad [S4]$$

where R is the radius of the unstretched droplet and a is the radius of the beads.

The measurement of viscoelasticity involved oscillating a trapped bead inside a settled droplet over a range of frequencies (0.5 to 40 Hz). The trap displacement amplitude was 1 μm up to 2.5 Hz and reduced to 0.5 μm at higher frequencies. The force trace at each frequency was fit to a sinusoidal function. The ratio of the force amplitude and the trap displacement amplitude, along with the corresponding phase shift, yielded the elastic and viscous moduli, denoted by $G'(\omega)$ and $G"(\omega)$, respectively, where ω is the angular frequency. Finally we fit the dependences of G' and $G"$ on ω to the Burgers model, given by eq [1] of the main text.

8. Monitoring droplet fusion by optical traps. Optical trap-directed droplet fusion was as described previously [3]. In short, two droplets trapped at minimum laser power (3%) were prepared as under "*Local melting of condensates inside focused laser beams*." The trap-1 droplet was then moved close to the trap-2 droplet. A snapshot of the two still separated droplets was taken (for determining pre-fusion droplet radius). Care was taken to align the traps horizontally. The trap-1 droplet was finally moved in steps of 10 to 20 nm until it came into contact with the trap-2 droplet, whereupon fusion proceeded spontaneously. The trapping forces, at a sampling rate of 78125 Hz, were recorded. The normalized trap-2 force was fit to eq [2] to yield the droplet fusion time.

9. Determination of condensate viscosity by single particle tracking. To prepare for single particle tracking, large, settled droplets (~20 μm in diameter) with a single bead inside were found. The bead was lifted by the trapping laser to be near the center of the droplet. A bright-field image of the bead was stored to serve as template. The trapping laser was then turned off and the bead was allowed to undergo free diffusion inside the droplet. The bead was tracked by template matching (at 15 Hz frame rate); tracking was stopped when the bead moved too far out of focus and lost matching with the template. The bead *x* and *y* positions along with the time stamps were exported as h5 file.

For each bead trajectory that was at least 800 s long, the mean-square-displacement (MSD) in the *xy* plane was calculated at lag times of 0.067 s to 120 s. The average of the MSD traces from six bead trajectories (acquired in different droplets) was fit to the relation

$$\mathrm{MSD} = 4Dt \quad [S5]$$

Finally the zero-shear viscosity η was obtained from the Stokes-Einstein relation

$$D = \frac{k_\mathrm{B}T}{6\pi\eta a} \quad [S6]$$

where k_B is the Boltzmann constant, T is the temperature in Kelvin, and a is the bead radius.

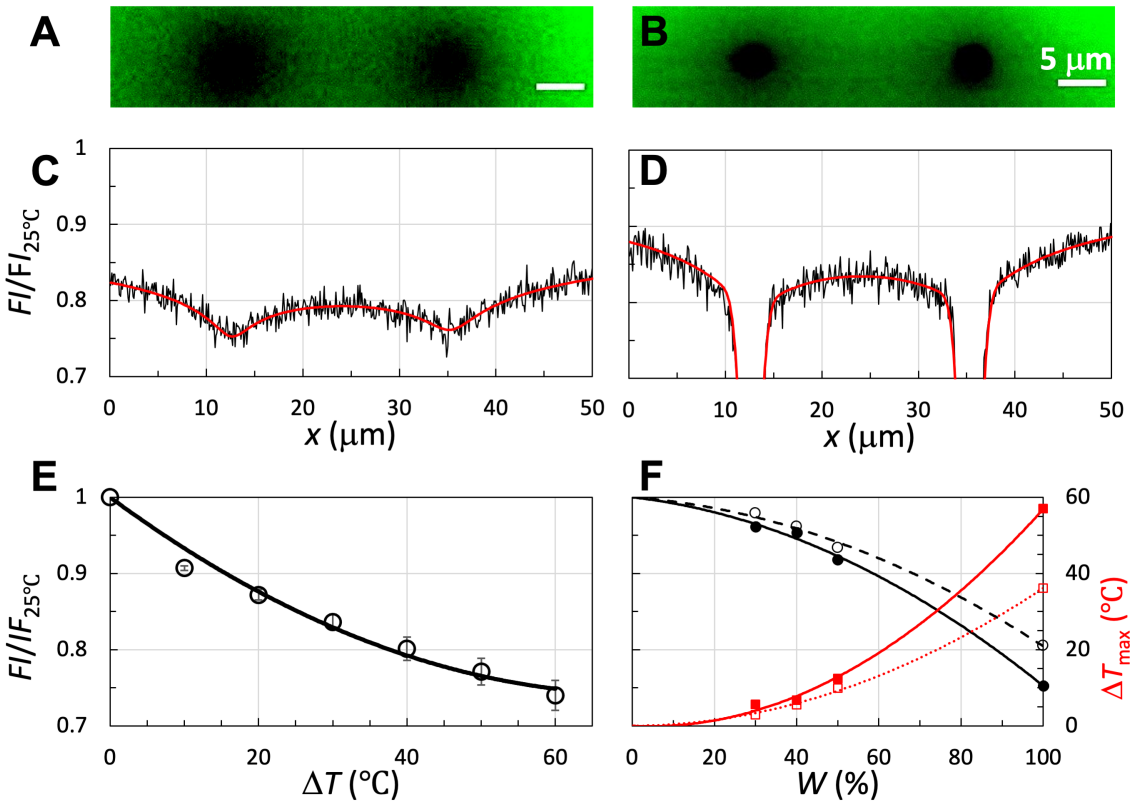

Figure S1. Calibration of the temperature jump due to the heating of focused laser beams. (A) Confocal image of buffer with 10 μM fluorescein, while illuminated by the two beams of the trapping laser at 100% power. (B) Corresponding image when the laser beams trapped two polystyrene beads. (C) Fit of the fluorescence intensity (black trace) from panel (A) at $y = y_c$ to eq [S1] (red curve). (D) Corresponding result for panel (B), with fit to eq [S2]. (E) The change in fluorescence intensity of a 10 μM fluorescein sample when the temperature was raised from 25 ºC, measured on a spectrofluorometer (excitation at 488 nm and emission integrated from 501 to 521 nm). Data are presented as mean ± standard error of the mean (N = 3); curve is the fit to a quadratic function, $FI/FI_{25ºC} = 5.015 \times 10^{-5}\ \Delta T^2 - 7.198 \times 10^{-3}\ \Delta T + 1$. (F) Left vertical axis (black symbols and curves): maximum reduction in fluorescence intensity, at the center of a laser beam without a trapped bead (filled circles) or at the surface of a trapped bead (open circles), at 30%, 40%, 50%, and 100% laser power. Solid and dashed curves are fits to a quadratic function. Right vertical axis (red symbols and curves): corresponding maximum temperature jumps (filled squares and solid curve for trapping laser with beads; open squares and dashed curve for trapping laser with beads).

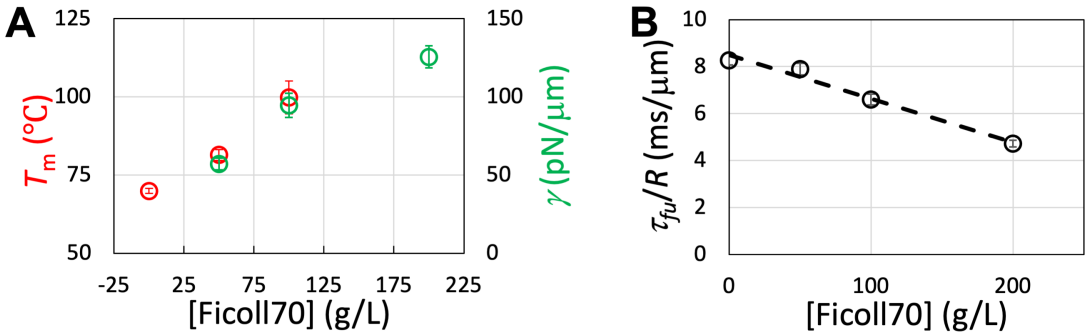

Figure S2. Effects of Ficoll70 on the thermodynamic and material properties of pK:H condensates. (A) Matching effects of Ficoll70 on the melting temperature and the interfacial tension. (B) Decrease in the inverse fusion speed at increasing Ficoll70 concentration.

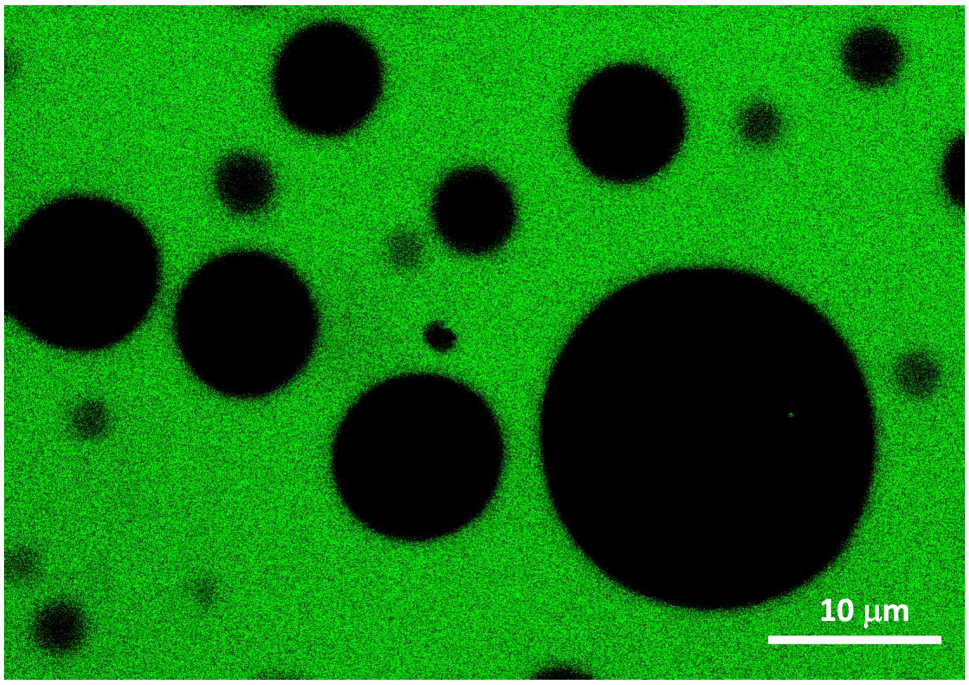

Figure S3. Exclusion of Ficoll70 from pK:H condensates, shown by a confocal image of a pK:H sample with 100 g/L of unlabeled Ficoll70 plus 5 µM FITC- Ficoll70.

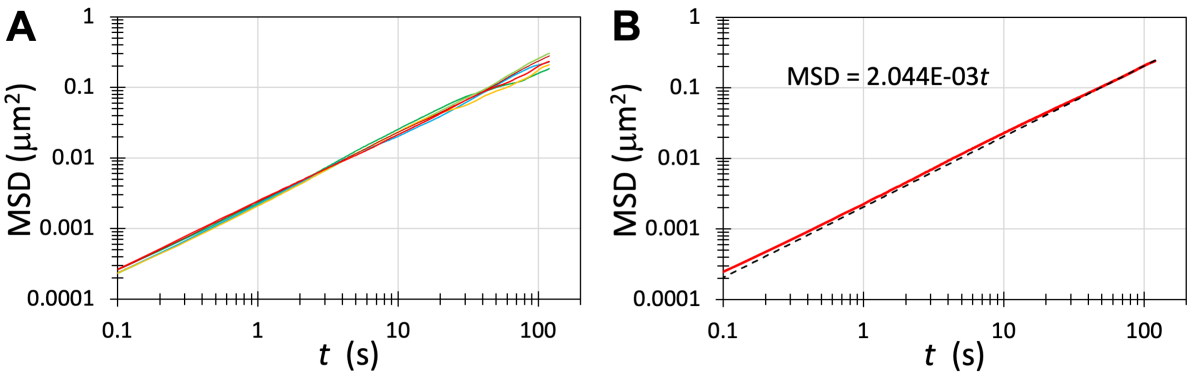

Figure S4. Determination of condensate viscosity by single particle tracking. (A) Mean-square-displacements (MSDs) of six beads each tracked for at least 800 s. (B) Average MSD, fit to a proportional relation with time. The slope, 2.044×10^{-3} μm²/s, yields a viscosity of 0.426 Pa s.

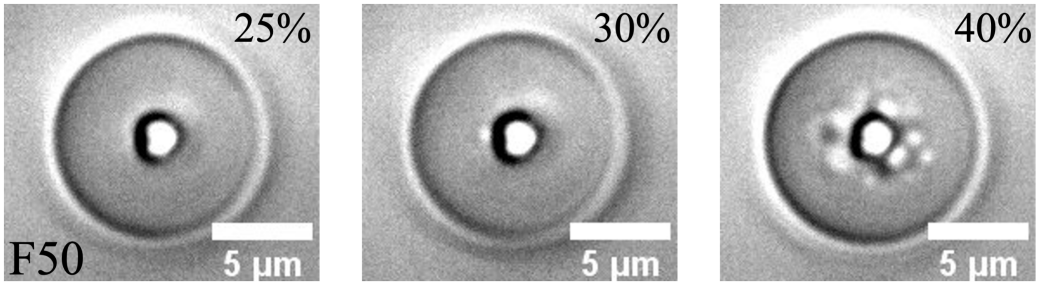

Figure S5. Bright-field images showing the local melting of pK:H condensates with 50 g/L Ficoll70, starting at 30% laser power when the laser beams trapped polystyrene beads.

References

1. Ghosh, A.; Kota, D.; Zhou, H. X. Shear Relaxation Governs Fusion Dynamics of Biomolecular Condensates. *Nat Commun* **2021,** *12*, 5995.

2. Zhou, H. X. Determination of Condensate Material Properties from Droplet Deformation. *J Phys Chem B* **2020,** *124*, 8372-8379.

3. Ghosh, A.; Zhou, H. X. Determinants for Fusion Speed of Biomolecular Droplets. *Angew Chem Int Ed* **2020,** *59*, 20837-20840.

Supporting Information Movie 1. Local melting of pK:H droplets due to temperature jump inside two focused laser beams. Ficoll70 is absent in the sample preparation. The droplets are trapped and suspended by the laser beams. The power of the laser beams is held alternatively at baseline (10%) and increasingly elevated (15% to 30%) levels for approximately 30 s each. At increasing elevation of the laser power, more and more bubbles emerge from inside the laser beams, which then fuse and pop at the rim of the droplets. Bubbles all disappear when the laser power is returned to the baseline level, except for the last time. In that case, in the droplet on the right side, small bubbles all fuse into a giant bubble, which squeezes the condensed phase, significantly expands the overall volume of the droplet, and persists till the end of the recording.

Supporting Information Movie 2. Local melting of pK:H droplets due to temperature jump inside two focused laser beams. 50 g/L Ficoll70 is present in the sample preparation. The power of the laser beams is held alternatively at baseline (15%) and increasingly elevated (20% to 40%) levels for approximately 30 s each. At increasing elevation of the laser power, more and more bubbles emerge from inside the laser beams, which then fuse and pop in the normal-temperature regions outside the laser beams. Bubbles all disappear when the laser power is returned to the baseline level.

Supporting Information Movie 3. Local melting of pK:H droplets due to temperature jump inside two focused laser beams. 100 g/L Ficoll70 is present in the sample preparation. The power of the laser beams is held alternatively at baseline (30%) and increasingly elevated (35% to 50%) levels for approximately 30 s each. At increasing elevation of the laser power, more and more bubbles emerge from inside the laser beams, which then fuse and pop in the normal-temperature regions outside the laser beams. Bubbles all disappear when the laser power is returned to the baseline level.